


Study on hydrogen smelting reduction behaviour in synthetic molten Hlsarna slag

Theint Theint Htet^a, Zhiming Yan ^a, Bharath Sampath Kumar^a, Johannes Hage^b, Koen Meijer^b and Zushu Li^a

^aWMG, University of Warwick, Coventry, UK; ^bIJmuiden Technology Centre, IJmuiden, The Netherlands

ABSTRACT

The reduction behaviour of hydrogen with FeO in synthetic molten Hlsarna slag has been investigated using two experimental methods: (1) Blowing 5% or 10% H₂-Ar onto the molten slag at 1450°C, 1475°C, 1550°C, respectively; and (2) Injecting 10% H₂-Ar into the molten slag at the flowrates of 0.5, 1.0, 1.5 L min⁻¹. During the gas blowing onto the melt, the reaction is initially controlled by gas phase diffusion, followed by limitation of liquid phase diffusion. The reaction rate is significantly improved by injecting the gas into the molten slag; bubbles are generated during the gas injection resulting in ample surface area between the gas and liquid slag. The overall reduction is controlled by the liquid phase mass transfer of FeO in the injection case; described by the penetration theory.

ARTICLE HISTORY

Received 30 November 2022
Revised 12 April 2023
Accepted 13 April 2023

KEYWORDS

Hlsarna process; hydrogen; smelting reduction; slag-gas reaction; kinetics; Mass spectrometer; mass transfer; penetration theory

Introduction

Global warming and climate change have become a significant problem due to the increasing level of greenhouse gases in the atmosphere. The steel industry is one of the major industrial CO₂ emitters, responsible for 6.5% of all the CO₂ emissions around the globe [1]. As a result, drastically reducing the carbon footprint has become a priority in the agenda of many industrial countries. In 2015, the Paris agreement was adopted to mitigate global warming, aiming to limit the global average temperature rise to below 2°C [2]. To meet the Paris climate target, the EU adopted a European Climate Law: the goal of reaching climate neutrality by 2050, following the European Green Deal, launched in 2019 [2]. However, it is challenging to achieve carbon-lean steel production and to meet the stringent environmental legislation [1,3] with the current technologies. Hence, research and development initiatives worldwide have been exploring alternative ironmaking technologies under CO₂ breakthrough programmes, which can accommodate a greener material in the process [4]. The Ultra-Low CO₂ Steelmaking (ULCOS) is one of the most extensive research programmes, jointly initiated by 15 European countries and 48 enterprises and supported by European Commission [4,5]. The Hlsarna process based on the smelting reduction process, and developed by Tata Steel, is one of the promising alternative ironmaking processes among ULCOS programme [5]. It aims to reduce CO₂ emissions through the process alone by 20% and by 80% when combined with carbon capture and storage (CCS) [4–7]. One of the main advantages of the Hlsarna process is providing a direct use of alternative reductants to the expensive metallurgical coal without any pre-treatment [8]. The pilot plant with the capacity of 60,000 t/a was set up by Tata steel in IJmuiden, and successfully demonstrated using alternative reductants such as thermal coal and charcoal [7–10]. This result creates an opportunity to explore the potential of the usage of different alternative reductants, other than solid materials.

There has been a great interest in using hydrogen in the ironmaking process due to its efficient reducing properties and its non-harmful products, i.e. water steam. Hence, various alternative ironmaking technologies using hydrogen have been developed around the globe to replace the carbon fully or partially in the process and reduce the CO₂ emission. In Sweden, the Hydrogen Breakthrough Ironmaking Technology (HYBRIT), a fossil-free steel making process, was co-founded by SSAB (a Swedish steel company), Vattenfall (an energy supplier) and LKAB (a Swedish mining company) in 2016 [9,10]. The main concept of the project is the direct reduction of iron ore by using 100% hydrogen produced by electrolysis. At present, iron ore direct reduction by hydrogen-rich gas has been industrialised, such as Midrex and Hylsa (HYL) processes, using natural gas, coal, and oil-gasified gas, in which hydrogen content is 55 vol.-% to 80 vol.-% [10]. Moreover, the research regarding hydrogen plasma reduction (HPR) based on smelting reduction is also in progress, as an alternative to the hydrogen direct reduction route [1].

The alternative iron making processes using hydrogen are being developed to mitigate the CO₂ emission, as a results, researchers focus on studying the fundamentals of the reduction reaction between iron oxide and hydrogen. Kawasaki et al. [11] conducted the direct reduction study on porous haematite pellets using hydrogen and carbon monoxide. The authors claimed that the reduction of solid iron oxides occurs in stepwise: haematite → magnetite → wustite → iron, and the rate is controlled by the equimolar counter diffusion of the reactant gas and the product gas [11]. A similar conclusion had been reached by Lin et al. [12] that iron oxide (Fe₂O₃) is reduced to Fe₃O₄, and finally to metallic iron. Moreover, the effect of hydrogen partial pressure on the iron ore pellet was examined by Qie et al. [13], and they reported that the overall rate increases with the hydrogen content, when hydrogen partial pressure is above 10%, and addition of hydrogen to the reductant gas mixture has a positive influence on the reduction reaction.

CONTACT Zhiming Yan  Zhiming.Yan@warwick.ac.uk; Zushu Li  z.li.19@warwick.ac.uk  WMG, University of Warwick, Coventry, CV4 7AL, UK

© 2023 The Author(s). Published by Informa UK Limited, trading as Taylor & Francis Group

This is an Open Access article distributed under the terms of the Creative Commons Attribution License (<http://creativecommons.org/licenses/by/4.0/>), which permits unrestricted use, distribution, and reproduction in any medium, provided the original work is properly cited. The terms on which this article has been published allow the posting of the Accepted Manuscript in a repository by the author(s) or with their consent.

On the other hand, Zhang et al. [13] investigated the reduction rate of copper slag pellet containing Fe_2SiO_4 and Fe_3O_4 ; the rate increases with the partial pressure of hydrogen, and it is controlled by the internal diffusion and chemical reaction.

In the early years, Ban-ya et al. [14] investigated gas/liquid system, i. e. the reduction behaviour of hydrogen with liquid wustite, and its reduction potential in various inert gases such as argon, nitrogen, and helium. The authors [14] reported that the reaction mechanism involved in the process, i.e. the overall reaction rate is limited by gas phase mass transfer in the range of flowrate $4\text{--}7\text{ L min}^{-1}$. Moreover, they claimed that the reaction between hydrogen and wustite is rapid. Nagasaka et al. [15] studied the interfacial kinetics of hydrogen with FeO bearing liquid slag, and suggested that it is advantageous to use hydrogen in a rapid reduction of liquid iron oxide in the bath smelting process since it provides a faster reaction compared to other reductants such as CO gas, solid carbon, and carbon dissolved in molten iron. Furthermore, research has been done on hydrogen plasma reduction kinetics (gas/liquid), as usage of pure hydrogen in the direct reduction furnace is challenging due to endothermic reaction [1,16,17]. The authors [1] claimed that the diffusion of oxygen species in solid state is no longer a rate-limiting step in plasma reduction, and the haematite is melted and reduced simultaneously. They also reported that the iron oxide reduction with hydrogen plasma is exothermic, unlike in direct reduction process. These past and ongoing research regarding using hydrogen in various alternative ironmaking processes leads to the current fundamental study on the reduction of iron oxides in molten Hlsarna slag with hydrogen.

The previous literature [1,11–13,16] provided the potential usage of hydrogen and its efficiency for iron oxide reduction, focusing mainly on using hydrogen in direct reduction process (solid state reduction) and plasma smelting reduction process, and very few [14,15] studied on smelting reduction kinetics. In the smelting reduction vessel of Hlsarna process, the iron oxide (FeO) in the molten slag could be reduced by predominantly carbon injected in different forms of thermal coal or charcoal, and by the hydrogen and CO in the gas phase. As a continuous study on the role of individual reductants (e.g. different carbons [18,19], hydrogen), this work studies the reduction behaviour of hydrogen with FeO in molten synthetic Hlsarna slag. In the present research, to determine the reduction behaviour of iron oxide in molten Hlsarna slag by hydrogen-containing gas, two types of experiments were carried out: (1) blowing $\text{H}_2\text{-Ar}$ onto the FeO-containing liquid Hlsarna slag at 1450°C , 1475°C and 1550°C respectively, (2) injecting $\text{H}_2\text{-Ar}$ into the liquid slag at 1550°C . The slag system investigated was $\text{FeO-SiO}_2\text{-Al}_2\text{O}_3\text{-MgO-CaO}$ with $6\text{--}12\text{ wt}\%$ FeO. The effect of partial pressure and flowrate of hydrogen, and the experimental methods on the reduction efficiency were investigated. The reaction mechanism involved in the two experimental methods was determined and the comparison of the reaction mechanism between the two methods is discussed in this study.

Experimental method

Materials

The high-purity powders of CaO, MgO, SiO_2 , Al_2O_3 (Sigma-Aldrich, 99.99%) and FeO (Sigma-Aldrich, 99.995%) were

used for making a synthetic slag, following the composition of Hlsarna slag after exclusion of minor components. The oxides powder of $\text{CaO-SiO}_2\text{-}13\text{ wt}\%\text{ Al}_2\text{O}_3\text{-}6\text{ wt}\%\text{ MgO-x wt}\%\text{ FeO}$ (binary basicity = 1.25, $x = 6, 9, 12$) were thoroughly mixed at room temperature and placed in an alumina crucible. During the experiment, the crucible containing oxides powder was slowly heated in argon atmosphere, to the reaction temperature resulting in a molten slag. Once the reaction zone reaches to the target temperature, the crucible was held for 30 min, ensuring homogeneity, before the reducing gas was blown or injected.

The Energy Dispersive Spectroscopy (EDS) method was used to determine the alumina content in the molten slag after the blowing (case 1) and injection experiments (case 2). It was found that the alumina content did not increase significantly during the blowing experiments (case1). On the other hand, a big increase in alumina composition was observed after the injecting experiment (case 2) due to dissolving of alumina lance into the molten slag during the injection. The composition of the reduced sample with $1.5\text{ L min}^{-1}\text{ H}_2\text{-Ar}$ injection is $25.8\text{ wt}\%\text{CaO-}25.1\text{ wt}\%\text{SiO}_2\text{-}40.4\text{ wt}\%\text{ Al}_2\text{O}_3\text{-}6.0\text{ wt}\%\text{ MgO-}2.5\text{ wt}\%\text{ FeO}$. However, the effect of increased alumina concentration in the slag could not be determined as case 1 and case 2 were conducted in different experimental methods. Hydrogen pressure of 0.05 and 0.1 atm in argon was selected for the current research.

Apparatus

A silicon carbide resistance vertical tube furnace (VTF) was used for isothermal gas reduction experiments. An illustrative diagram of the experimental set-up is shown in Figure 1. The top and bottom ends of VTF (inner diameter $88\text{ }\phi\times\text{length } 1060\text{ mm}$) were equipped with water-cooled flanges to protect the O-rings. A tapered alumina crucible ($31\phi\times 25\phi\times 45\text{ mm}$) containing oxides mixture was placed in the hot zone of the furnace. A B-type thermocouple was located just beneath the sample crucible to obtain the temperature of the reaction zone. An alumina lance (ID: 5 mm) was positioned 10 mm above the melt for the gas-blowing case, whereas the lance was immersed 5 mm into the melt for the injection case.

The exhaust gas composition was monitored throughout the reaction using online gas Quadrupole Mass Spectrometer (QMS) (HPR20, HIDEN Analytical) for kinetic analysis. A non-return valve was fitted to the exhaust line as in Figure 1 to prevent from backflow of the air into the furnace.

Experimental procedure

An alumina crucible containing 10 g of slag with 6 wt-% FeO was placed in the hot zone of the VTF. The furnace tube was filled with argon (N5, 99.999%) at the flow rate of 1 L min^{-1} through the bottom gas inlet, and a complete inert atmosphere inside the furnace was achieved within 10 min. The furnace was heated to the selected temperatures of 1450°C , 1475°C and 1550°C with the heating rate of $12^\circ\text{C min}^{-1}$ for the isothermal reduction experiments. Once the reaction zone achieved the target temperature, the temperature was maintained within $\pm 5^\circ\text{C}$ throughout the experiment. At the selected reaction temperature, the sample was kept isothermally for 30 min in inert atmosphere before introducing the reaction gas, ensuring sample homogeneity. Then, 5

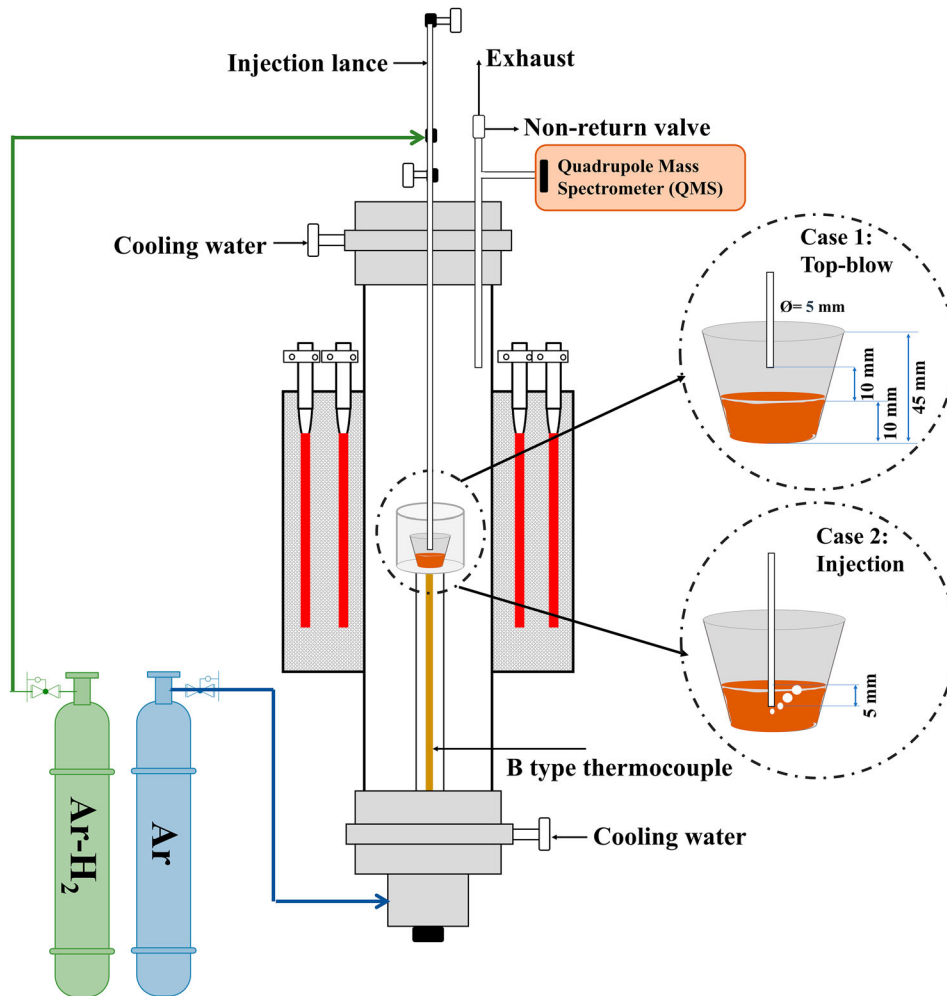


Figure 1. An illustrative diagram of the experiment setup for smelting reduction of FeO by H₂-Ar.

and 10 vol.-% of H₂ in argon was introduced from the top alumina lance. The current study involved two main methods:

- (1) **Case 1 (blowing):** 5 or 10 vol.-% H₂-Ar was blown from the lance located 10 mm above the molten slag surface, onto the molten slag for 1500 s with the flowrate of 1 L min⁻¹ at 1450°C, 1475°C, 1550°C. Concurrently, argon entered the furnace from the bottom gas inlet at a flowrate of 1 L min⁻¹, as shown in Figure 1. This bottom flow of argon was the carrier for the off gas, as well as a diluent for hydrogen inside the furnace. To determine the reduction kinetics, the off-gas composition, particularly moisture, was monitored by QMS throughout the experiment. Furthermore, case 1 with 10 vol.-% H₂-Ar at 1550°C was repeated with 9 and 12 wt.-% FeO in molten slag to determine whether the overall reduction was controlled by gas phase diffusion or liquid phase mass transfer.
- (2) **Case 2 (injection):** To study the effect of the surface area between gas and liquid slag on the overall reduction rate, case 2 was performed. 10 vol.-% H₂-Ar was injected into the molten slag with varied flowrates of 0.5, 1.0, and 1.5 L min⁻¹ at 1550°C. During the experiment, the alumina lance was lowered slowly and eventually inserted into the molten slag, followed by the gas flow for 2000 s, while the carrier gas, argon with 1 L min⁻¹ was flowing from the bottom gas inlet. After 2000 s, the gas flow stopped, and the lance was taken from the

melt to prevent further dissolution of the lance into the slag. Figure 1 shows the lance position for both case 1 and case 2. Like in case 1, the off-gas composition is recorded by QMS for the kinetic analysis.

In both cases, the reaction gas, H₂-Ar was turned off immediately once the residence time was over, and the furnace was rapidly cooled within 15 min from the reaction temperature to the solidus temperature of the slag. This is to ensure that there was no further alumina dissolution from the crucible during the cooling stage, and to obtain the slag sample for further analysis, whose condition was as close as the one during the reaction.

Results

The evolved gas composition recorded by QMS

Since water is generated from the reaction between FeO in molten slag and H₂, the reduction rate of FeO in the molten slag can be calculated from the rate of water generation. Hence, FeO reduction kinetics is studied based on the off-gas composition recorded by QMS. The off-gas composition obtained from QMS during the blowing of H₂-Ar onto the molten slag bath is shown in Figure 2(a,b). According to Figure 2(a), the water concentration in the off-gas increases with the increasing reaction temperature in the case of 5 vol.-% H₂-Ar, while the case of blowing 10 vol.-% H₂-Ar does not fully follow the similar trend (Figure 2(b)).

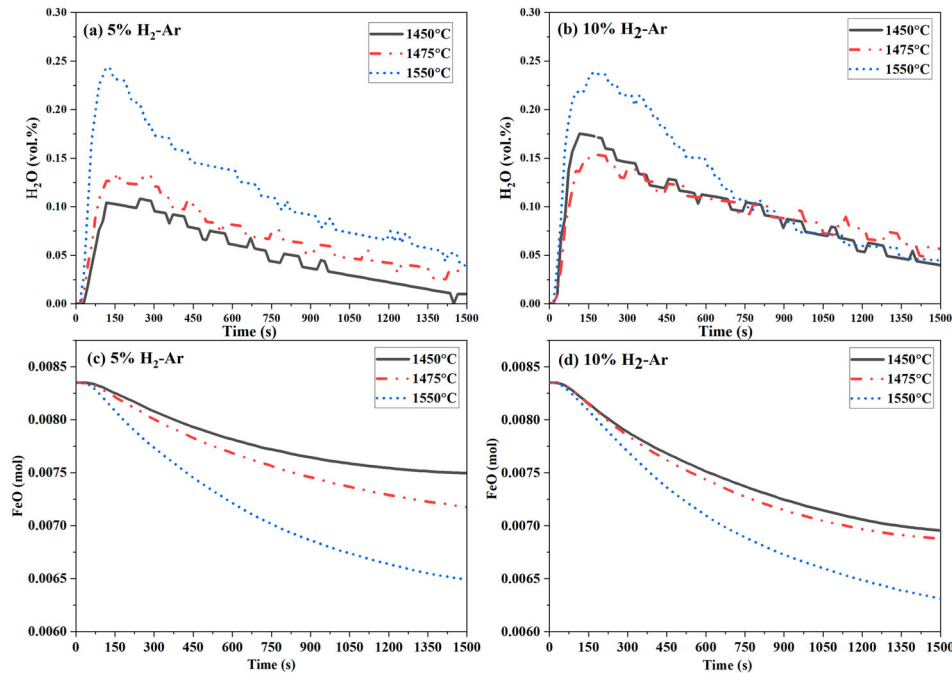
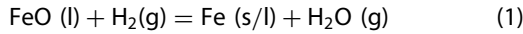


Figure 2. The H₂O (vol.%) in off-gas obtained from QMS during the blowing of (a) 5% H₂-Ar and (b) 10% H₂-Ar, and the calculated FeO (mol) in the molten slag during the blowing of (c) 5% H₂-Ar and (d) 10% H₂-Ar at different temperatures.

The amount of FeO (mol) in molten slag during the reaction is determined from Figure 2(a,b), as the amount of water evolved during the reaction in mol is the same with the amount of FeO reduced in mol according to stoichiometric Equation (1). The calculated moles of FeO in the molten slag during the reduction are shown in Figure 2(c, d). According to Figure 2(c,d), the FeO reduction rate is directly proportional to the increasing temperature and vol.-% H₂ in argon.



Determination of reduction degree for gas blow and injection cases

The degree of FeO reduction during the reduction with 5 and 10 vol.-% H₂ at the temperature range of 1450–1550°C is determined using Equation (2). The calculated reduction degree results are presented in Figure 3(a,b).

$$\alpha = \frac{\text{FeO}_i - \text{FeO}_t}{\text{FeO}_i} \quad (2)$$

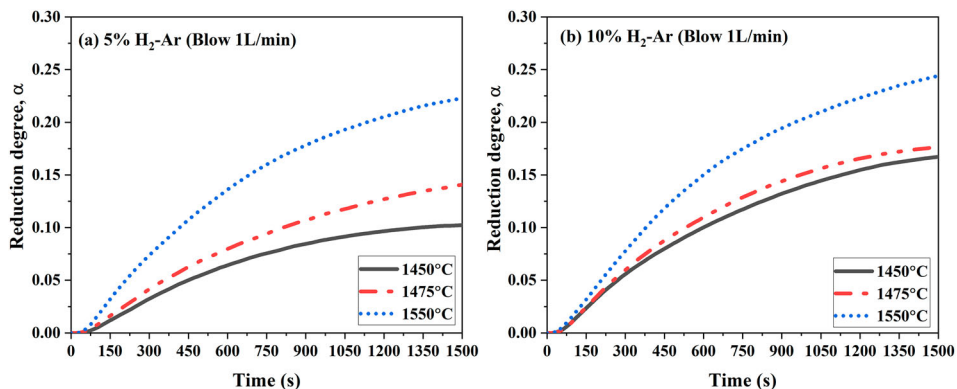


Figure 3. The calculated reduction degree of FeO during the reaction (blowing) with (a) 5% H₂-Ar, and (b) 10% H₂-Ar.

where α represents reduction degree; FeO_i and FeO_t are the amount of FeO in mole at the initial condition and at the time t , respectively.

The reduction degree and overall reduction rate increase with the increasing temperature, and the maximum reduction degrees achieved at 1550°C from the reduction with 5% and 10% H₂-Ar are 0.22 and 0.24, respectively, according to Figure 3(a,b). The values are significantly increased in the case of injecting 10% H₂-Ar into the molten bath, as shown in Figure 4. The maximum reduction degrees of 0.31, 0.45 and 0.54 after injection for 2000 s are achieved during the injection of 10% H₂-Ar at 1550°C with a flowrate of 0.5, 1, and 1.5 L min⁻¹, respectively. Hence, the gas injection method provides a higher overall reduction rate and reduction degree compared to directly blowing the gas onto the molten bath.

Effect of the FeO content during the blowing of H₂-Ar onto the molten slag

To determine the reaction mechanism between molten slag and the gas of case 1, gas-blowing experiments are repeated

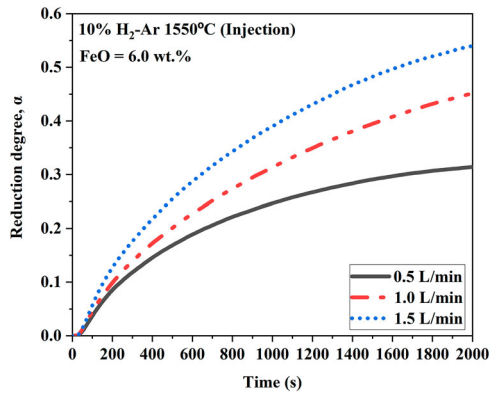


Figure 4. The calculated reduction degree of FeO during the injection of 10% H₂-Ar into the molten slag at different gas flow rates.

using 10 vol.-% H₂-Ar at 1550°C with the slag containing 6.0–12.0 wt-% of FeO. The reduction degree curves of varied FeO wt-% in the molten slag are presented in Figure 5. The FeO reduction rate remains similar during the initial 600 s of the reaction although the FeO concentration in the slag varied from 6.0 to 12.0 wt-%, as shown in Figure 5. After 600 s, the reduction curves diverge according to the FeO content in the liquid slag. This shows that the initial 600 s of the reaction is controlled by the gas diffusion (Region I), whereas the reaction is governed by the liquid diffusion (Region II) beyond 600 s due to the rate being dependent on the FeO content in the slag.

Discussion

The reduction of FeO in molten slag using hydrogen is studied kinetically in this section based on two scenarios: (1) Case 1: blowing H₂-Ar onto the molten slag; (2) Case 2:

injecting H₂-Ar into the molten slag. The overall reduction of FeO in molten slag using H₂-Ar could be expressed by Equation (1). The reaction mechanisms of both scenarios are discussed in section A and B, followed by optical micrographs, SEM images and schematic diagrams, presented in Figure 6 and Figure 10.

Case 1: Kinetics analysis for H₂-Ar blowing onto the molten slag

Once the H₂-Ar is blown onto the molten slag surface, a gas channel is formed as shown in Figure 6(a) due to a constant gas impinging on the bath throughout the reaction time. Hence, the main contact area between the gas and the slag would be the channel. Then the following mechanism might occur during the reduction process, and it is explained schematically in Figure 6(b).

- (i) Diffusion of H₂ in the gas phase to the gas/slag interface.
- (ii) Diffusion of FeO in the liquid slag phase to the slag/gas interface.
- (iii) Chemical reaction between H₂ and FeO at the slag/gas interface, producing Fe and H₂O.
- (iv) Once a layer of iron products is formed at the gas/slag interface, the iron layer sinks or move away from the gas/slag interface as shown in Figure 6(a1)- (a3) and (b). Then, a new surface area is replenished between slag and gas, hence there is a constant contact between the slag and gas.
- (v) Escaping of reaction product H₂O from the gas/slag interface through the channel into the gas bulk. Irons are not found at the top side of the channel Figure 6 (a3), showing that there might be less contact between H₂ and slag due to H₂O.

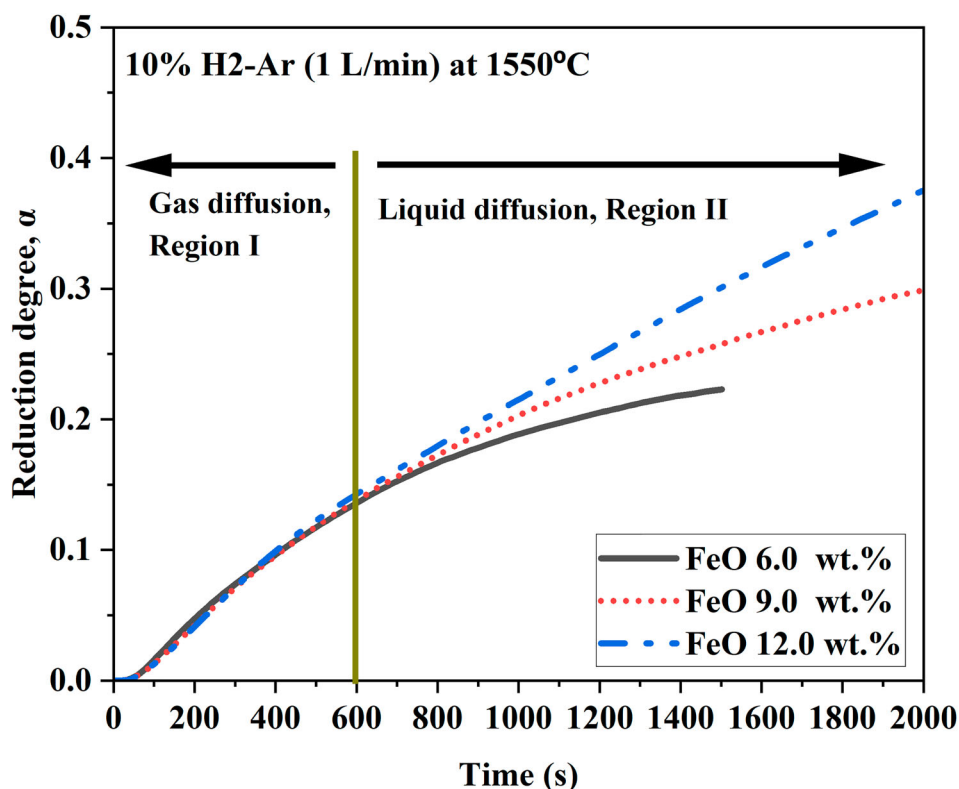


Figure 5. FeO reduction degree obtained when blowing 10% H₂-Ar onto the surface of the molten slags containing 6.0, 9.0 and 12.0 wt-% FeO at 1550°C.

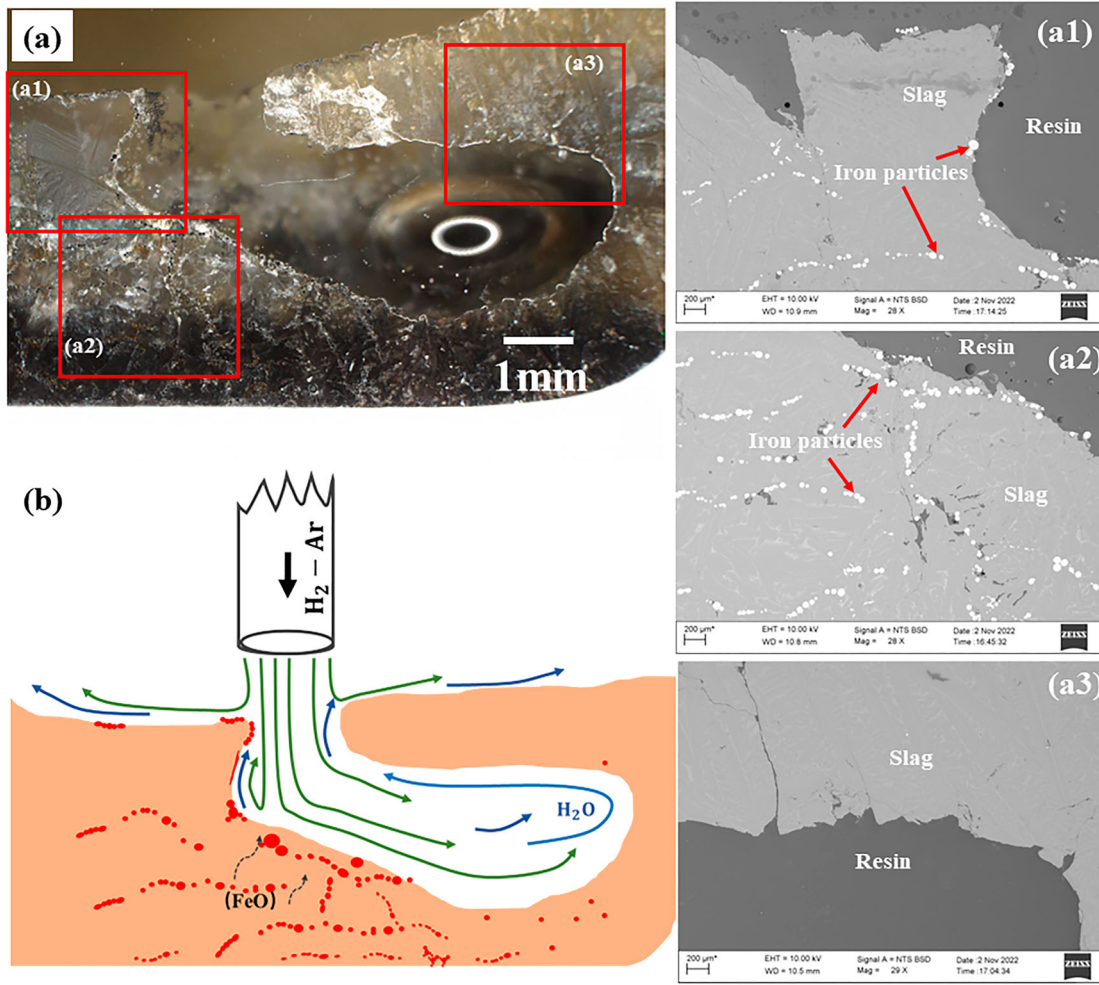


Figure 6. Reaction mechanism case 1: (a) Optical micrograph of slag (cross-section); (a1), (a2), and (a3) SEM images of the quenched slag; (b) schematic diagram showing the reaction mechanism.

It was confirmed that Region I (Figure 5) is controlled by H₂ diffusion to the gas/slag interface based on the experiment results, This implies that the FeO reduction rate could be significantly affected by the partial pressure of H₂ during the initial 600 s of the reaction [20]. For a gas phase mass transfer control, the flux of H₂ to the surface of liquid slag is given in Equation (3), according to the film theory [21–23].

$$J_{H_2} = \frac{k_G}{RT} \ln[1 + P_{H_2}] \quad (3)$$

where J_{H_2} represents the flux of the H₂ to the surface of the liquid slag (mol m⁻²·s); k_G is the rate constant (m/s); R is the gas constant (J mol⁻¹·K); T is the temperature (K); and P_{H_2} is the partial pressure of hydrogen in the gas phase (Pa).

It is acceptable to assume that the flux of H₂ (mass transfer of H₂ in gas phase) is equal to the FeO reduction rate during initial 600 s since it is the gas phase mass transfer region. The relationship between the rate and the partial pressure of H₂ is displayed in Figure 7. It is apparent that the reduction rate is increased with the increasing partial pressure of H₂ at all the reaction temperatures according to Figure 7. This is as expected from Equation (3). This further proves that the reaction is controlled by the gas phase mass transfer of hydrogen during the first 600 s of the reaction. In addition, the rate constant, k_G can be determined from Equation (3).

Once the equilibrium partial pressure of hydrogen is attained at the reaction interface, the reaction control step switches from gas phase diffusion control to liquid phase

diffusion control. Owing to liquid phase diffusion being dominant in Region II, a three-dimensional diffusion model known as the Jander equation is used to ascertain the liquid phase mass transfer rate constant, k_L [24,25]. The rate constant is determined using the integrated kinetic model Equation (4).

$$g(\alpha) = [1 - (1 - \alpha)^{1/3}]^2 = k_L t \quad (4)$$

where k_L is the liquid phase mass transfer rate constant (s⁻¹).

According to Figure 8, there is a good linear relationship in the plots at the temperature range of 1450–1550°C with the R^2 values of above 0.99 in both cases, 5% and 10% H₂-Ar. This implies that Region II could be described by the three-dimensional diffusion model. The kinetic parameters obtained from both Regions I and II are presented in Table 1.

According to Table 1, the rate constants, k_G and k_L increase with the temperature as well as with the partial pressure of hydrogen. This shows that the overall reaction is influenced by the increasing temperature and hydrogen partial pressure, while Region II is dominated by FeO diffusion in the liquid slag.

The activation energy values of Regions I and II of case 1 are determined through Arrhenius plots based on Equation (5) and presented in Figure 9(a) Region I, and (b) Region II, respectively. In both regions, activation energy values decrease with the increased partial pressure of hydrogen, indicating that a faster reaction rate is achieved with the

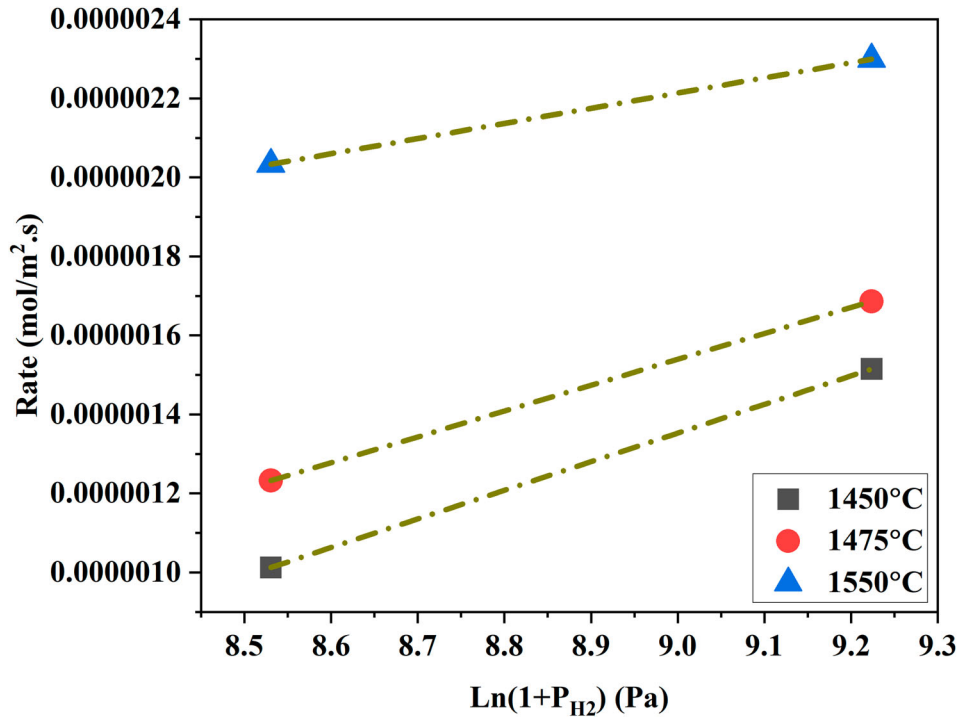


Figure 7. The variation of the FeO reduction rate as a function of the H₂ partial pressure at different temperatures in Region I.

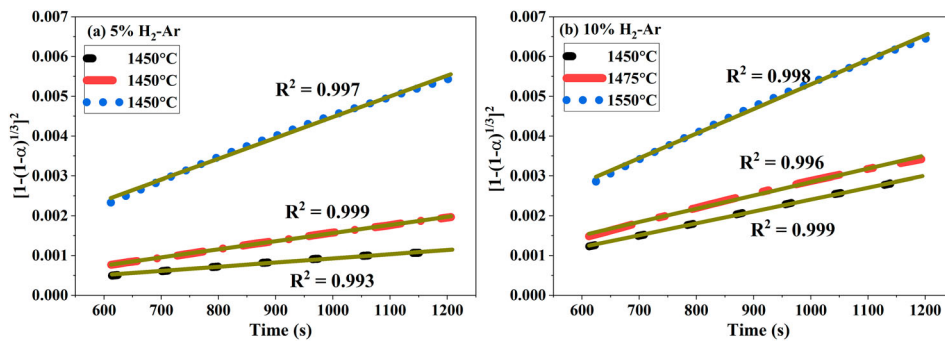


Figure 8. Linear curve fittings of the three-dimensional diffusion model in Region II to determine the mass transfer rate constants k_L (a) 5 vol.-% H₂-Ar, (b) 10 vol.-% H₂-Ar.

increased hydrogen partial pressure.

$$\text{Ln}k = \frac{-\Delta E}{RT} + \text{Ln}A \quad (5)$$

where k is the apparent rate constant, and it encompasses both k_G and k_L in this study, A and E are the pre-exponential factor and activation energy, respectively, and R is universal gas constant.

The values of 195 and 124 kJ mol⁻¹ resulted from reactions with 5% and 10% H₂-Ar in Region I (Figure 9(a)), whereas the values of 400 and 199 kJ mol⁻¹ were achieved

Table 1. Kinetic parameters obtained from gas and liquid phase diffusion regions.

H ₂ -Ar	Temperature (°C)	Gas phase diffusion Region I $k_G \times 10^{-3} (\text{ms}^{-1})$	Liquid phase diffusion Region II $k_L \times 10^{-6} (\text{s}^{-1})$
5% H ₂ (blowing)	1450	1.70	1.05
	1475	2.10	2.04
	1550	3.61	5.23
10% H ₂ (blowing)	1450	2.35	2.98
	1475	2.66	3.32
	1550	3.78	6.23

from reactions with 5% and 10% H₂-Ar in Region II (Figure 9(b)). In general, a lower activation energy will result in faster reaction rate. Hence, the reduction reaction in the gas diffusion region (Region I) is faster than that in the liquid diffusion region (Region II).

Case-2: Kinetics analysis based on 10% H₂-Ar injecting into the molten slag at 1550°C

To investigate the effect of surface area between gas and the molten slag on reaction, a gas injection experiment was conducted. During the injection of H₂-Ar into the molten slag, the reaction would mainly occur between the bubbles and FeO in the molten slag [26,27]. The detailed reaction mechanism for the case of gas injection is described as follows and it is schematically presented in Figure 10(c).

- (i) The small H₂-Ar gas bubbles are formed at the outlet of the injection lance.
- (ii) The hydrogen diffuses in the gas boundary layer of the individual bubble and reaches the gas/slag interface.

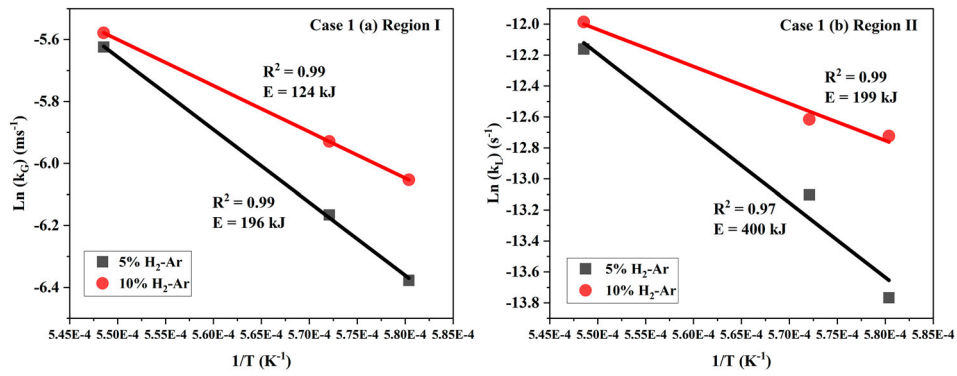


Figure 9. Determination of activation energy of (a) Region I, and (b) Region II.

- (iii) Fe^{2+} diffuses in the molten slag and reaches the gas/slag interface of each bubble.
- (iv) The H_2 -Ar bubbles react with Fe^{2+} at gas/slag interface.
- (v) Product irons are formed at the surface of the bubbles. The constant stirred slag bath leads to breakage of the bubbles, and coalescence of the iron into a large iron particle or pool followed by sinking to the bottom of the crucible due to its density, **Figure 10(a,b)**.
- (vi) H_2O product diffuses away from the slag/gas interface of each bubble, floats to the top of the bath, and eventually escaping into the bulk gas, **Figure 10(c)**.

In the case of the bubble/liquid reaction, the chemical reaction and gas diffusion steps are known to be rapid, hence the rate-controlling step would be the mass transfer of FeO in the liquid slag, step (iii) [26,28,29]. The results of FeO reduction at constant temperature, 1550°C and different gas flowrate are shown in **Figure 11** and the reaction

is determined using second order reaction equation that depicts the inverse of FeO content in the molten slag ($1/\text{FeO}$) vs time (Equation (7)).

$$-\frac{d[\text{FeO}_t]}{dt} = k_L \text{FeO}_t^\phi \quad (6)$$

$$\text{Second order reaction: } \frac{1}{\text{FeO}_t} = k_L t + \frac{1}{\text{FeO}_i} \quad (7)$$

where ϕ is the order of the reaction; k_L is the liquid phase mass transfer rate constant ($\text{mol}^{-1}\text{s}^{-1}$).

A linear relation between $1/\text{FeO}$ and time is observed with the R^2 values of above 0.98, according to **Figure 11**, indicating that the reaction is of second order, Equation (7). The apparent reaction rate constants for gas injection case, k_{inj} at different flowrate are determined through the curve fitting, **Figure 11** and presented in **Table 2**.

According to **Table 2**, the more intense the injected gas, the higher the reaction rate constant, k_{inj} is achieved. This further proves that the overall reduction is controlled by

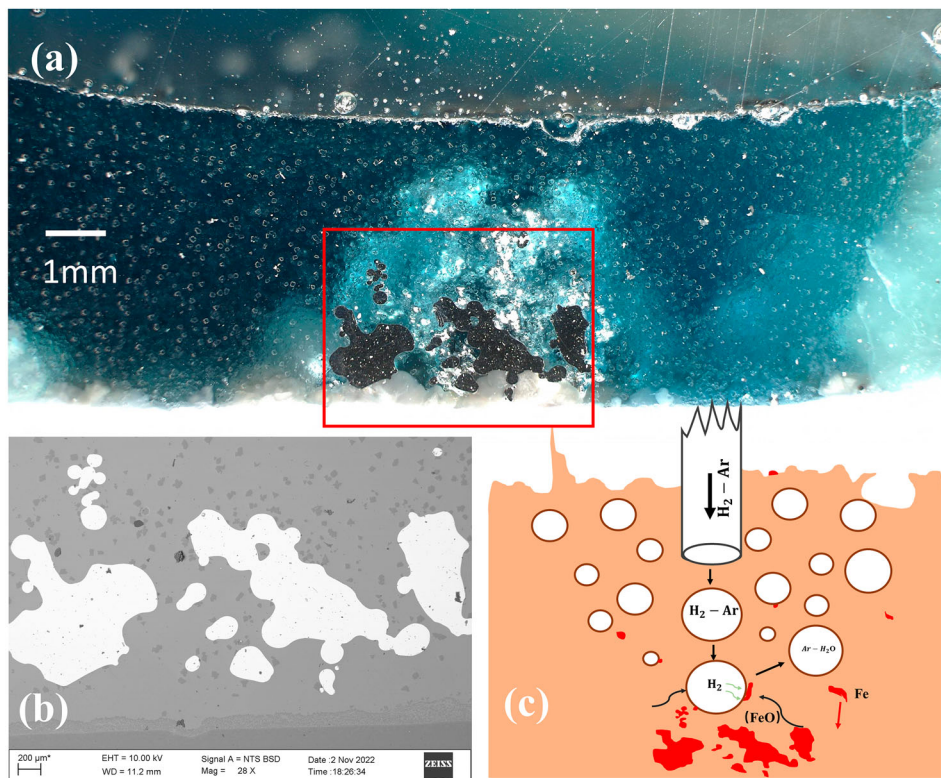


Figure 10. Reaction mechanism between the hydrogen gas bubbles and the molten slag during gas injection (a) Optical micrograph of sample cross-section, (b) SEM image, and (c) schematical diagram of bubble/molten slag reaction.

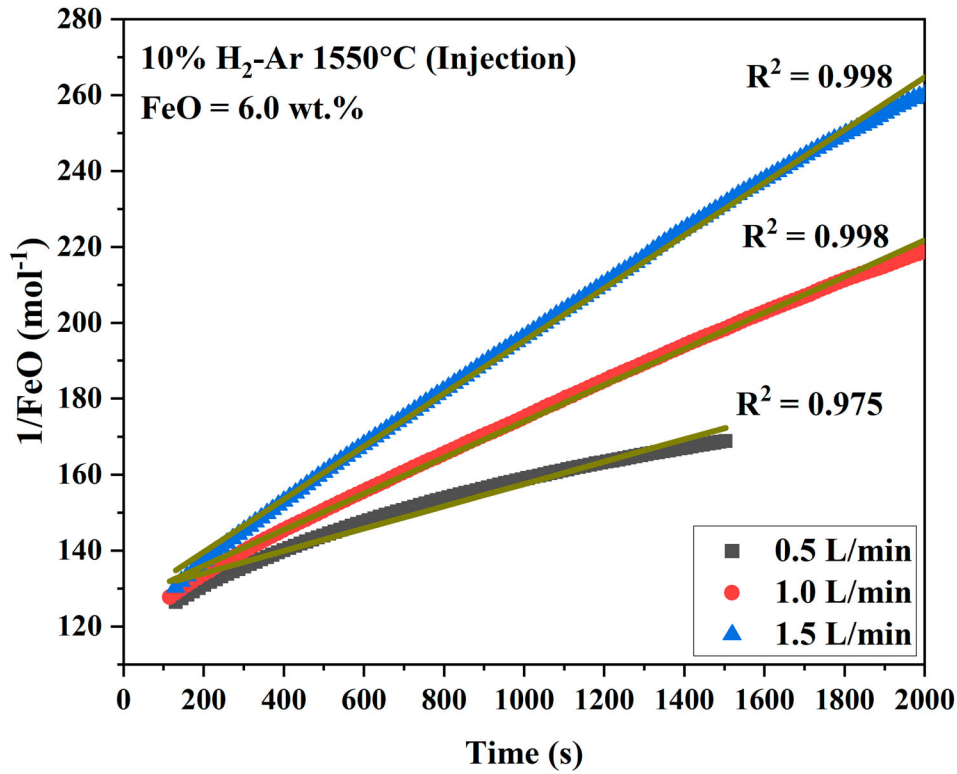


Figure 11. Determination of the liquid phase mass transfer rate constants of case 2, k_{inj} at different gas flowrates.

Table 2. Kinetic parameters obtained for injection of 10% H_2 -Ar into the molten slag.

	Flowrate (L min ⁻¹)	Reaction rate constant, $k_{inj} \times 10^{-2}$ (mol ⁻¹ s ⁻¹)
10% H_2 (Injection)	0.5	2.92
	1.0	4.75
	1.5	6.94

the diffusion of FeO in the liquid slag. Moreover, the more bubbles of similar diameter being generated with the increasing gas flowrate, creating a higher surface area between the bubbles and molten slag. This could be due to the higher convective mass transfer rate caused by the increasing gas flowrate, as well as more bubbles of similar diameter being generated resulting in higher surface area between the bubbles and molten slag.

The FeO mass transfer in the liquid slag could be described by Fick's law of diffusion, Equation (8) [28–30]

$$J_{FeO} = k_{FeO} (FeO_b - FeO^*) \quad (8)$$

where J_{FeO} is the mass transfer flux (mol m⁻²s); k_{FeO} is a mass transfer coefficient of FeO (m s⁻¹); FeO_b is the concentration of FeO in the slag bulk (mol m⁻³); FeO^* is the concentration of FeO at the gas/liquid interface (mol m⁻³).

According to the penetration theory [26,28,30], the mass transfer coefficient could be expressed as:

$$k_{FeO} = 2\sqrt{\frac{D_{FeO}}{\pi t_e}} \quad (9)$$

where D_{FeO} is the diffusion coefficient of FeO in the liquid film (m² s⁻¹), and t_e is a contact time between gas bubbles and the molten slag during gas injection (s).

k_{FeO} could be replaced by k_{inj} as the migration of Fe ions in the molten slag is the control step in the current research [26,27].

The contact time, t_e could be determined using Equation (10) [27,28]:

$$t_e = \frac{d_b}{v} \quad (10)$$

where d_b is an equivalent diameter of the gas bubble (m); and v is a velocity of the rising gas bubble (m s⁻¹).

Since the gas flow is low in the current study, the bubble size could be determined by the equilibrium of buoyant force and interface tension, on the assumption that the bubbles are spherical [26].

$$\frac{\pi d_b^3 g}{6} (\rho_l - \rho_g) = \pi d \sigma_l \quad (11)$$

where d is the diameter of the injection lance (m); ρ_l and ρ_g are the density of the liquid and gas (kg m⁻³), respectively; σ_l is the liquid surface tension (N m⁻¹).

The bubble rising velocity could be obtained from Stokes' formula as follows:

$$v = \frac{d_b^2}{12\mu_l} g (\rho_l - \rho_g) \quad (12)$$

where μ_l is the viscosity of the molten slag (Pa.s).

Density and the surface tension of the liquid slag are estimated according to Mills model [31], whereas, viscosity of the molten slag and gas density of the gas are obtained from Factsage (FactSage 8.2, GTT-Technologies and Thermfact/CRCT, 2022) calculation. Furthermore, diffusivity of FeO in liquid phase is calculated from Equation (8). However, the physical parameters varied during the injection experiments due to the dissolution of the alumina injection lance into the liquid slag. Hence the physical parameters were calculated with the slag composition achieved at the end of the 1.5 L min⁻¹ experiment, which provided the maximum alumina content in the slag. Table 3 summarises the

Table 3. Physical parameters of the slag at 1550°C under different flowrate.

13 wt-% alumina in slag					
Flowrate (L min ⁻¹)	μ_l (Pa.s)	ρ_l (kg m ⁻³)	ρ_g (kg m ⁻³)	σ_l (N m ⁻¹)	D_{FeO} (m ² s ⁻¹)
0.5					5.22×10^{-6}
1.0	0.146	2815	0.241	0.495	1.38×10^{-5}
1.5					2.95×10^{-5}
40 wt-% alumina in slag					
Flowrate (L min ⁻¹)	μ_l (Pa.s)	ρ_l (kg m ⁻³)	ρ_g (kg m ⁻³)	σ_l (N m ⁻¹)	D_{FeO} (m ² s ⁻¹)
0.5					2.84×10^{-5}
1.0	0.804	2822	0.241	0.51	7.52×10^{-5}
1.5					1.61×10^{-4}

parameters of the Hlsarna slag with 13 wt-% alumina content and the slag sample after the reduction with 1.5 L min⁻¹ injection rate. It is found that the viscosity of the slag was significantly increased with increasing the alumina content in the slag after the reduction test.

The mass transfer coefficient, in this case, k_{inj} is dependent on the physical properties of the fluid; this could be described by the following empirical equation, Equation (13) [26,32]:

$$Sh = m Re^{m1} Sc^{m2} \quad (13)$$

where Sh is the Sherwood number; Re is the Reynold's number; Sc is the Schmidt number; m , $m1$, $m2$ are constants. These parameters are described as follows [21,28] and the calculated values are shown in Table 4.

$$Sh = \frac{k_{inj}d_b}{D} \quad (14)$$

$$Re = \frac{v_o \rho_l d_b}{\mu_l} \quad (15)$$

where v_o is velocity of the injected gas (m/s).

$$Sc = \frac{\mu_l}{\rho_l D_{FeO}} \quad (16)$$

The constants of the Sherwood correlation were regressed in the current study, Equations (17) and (18).

$$Sh = 13.92 Re^{0.01} Sc^{0.5} \rightarrow (13.Wt.\%alumina \text{ in slag}) \quad (17)$$

$$Sh = 2.7 Sc^{0.5} \rightarrow (40wt.\%alumina \text{ in slag}) \quad (18)$$

According to Table 4, the Sherwood number decreased when the alumina composition was 40 wt-% in the sample due to the increasing viscosity of the liquid slag. Since the dissolution of alumina into the slag was not the focus of this study, the diffusion coefficient of alumina into the slag or the amount of alumina in the slag during the reduction period was not monitored, apart from the final alumina content in the slag after the reduction experiment with 1.5 L min⁻¹ injection rate. According to Equations (17) and (18), when the alumina is 40 wt-% in the slag, the Sherwood number decreases by a factor of 5 times compared to the slag with 13 wt-% alumina. It should also be noted that during the analysis of the data for the 40 wt-% case, the Reynold's number becomes statistically insignificant and has no impact on the mass transfer process, as shown in Equation

(18). This shows that the convective mass transfer rate decreases with the increasing viscosity of the liquid slag and the molecular diffusion becomes dominant. The overall reduction rate might not be significantly impacted by the convective mass transfer rate. Conversely, it is improved with the increased surface area between gas and liquid slag generated by the increasing gas flowrate, while the liquid phase mass transfer of FeO (molecular diffusion) could still be the limiting step.

Conclusion

The rate of FeO reduction in synthetic molten Hlsarna slag by H₂-Ar was studied using two cases, and the following conclusions could be made:

In the case of blowing H₂-Ar onto the molten slag at different temperature and partial pressure of H₂, the reduction rate of FeO in liquid slag increases with increasing reaction temperature and partial pressure of hydrogen. The overall reduction process is controlled by two main steps; first, the diffusion of H₂ in the gas phase, during the initial 600 s (Region I) of the reaction, and second, by the diffusion of FeO in the liquid slag, which becomes dominant beyond 600 s (Region II) of the reaction.

In the case of injecting 10% H₂-Ar into the molten slag at 1550°C with varied flowrate, the overall reduction rate is increased by increasing gas flowrate. The higher the gas flowrate, more bubbles are dispersed in the molten slag, leading to more reaction surface area between gas and slag. Hence, the surface area has a significant effect on the reduction rate. The mass transfer process is explained in a dimensionless analysis, and it is found that the reaction rate is not significantly influenced by the gas flow velocity, as the Reynold's number contribution is negligible, instead it is significantly affected by the increased bubbles generation due to the increased flowrate, which could ultimately improve the molecular diffusivity in the liquid slag.

Acknowledgements

Theint-Theint Htet highly appreciates Tata Steel Europe in Umuiden for the full PhD studentship. Zushu Li would like to acknowledge the financial support from EPSRC under grant number EP/N011368/1 (EPSRC Fellowship).

Disclosure statement

No potential conflict of interest was reported by the author(s).

Funding

This work was supported by Engineering and Physical Sciences Research Council [grant number EP/N011368/1].

Table 4. Dimensionless number for the interfacial mass transfer process.

Flowrate (L min ⁻¹)	13 wt-% alumina in slag			40 wt-% alumina in slag		
	Sh	Re	Sc	Sh	Re	Sc
0.5	45.45	6.66	9.93	8.43	12.22	10.02
1.0	27.94	13.31	3.75	5.18	24.44	3.79
1.5	19.12	19.96	1.76	3.55	36.66	1.77

ORCID

Zhiming Yan  <http://orcid.org/0000-0002-6061-4077>

References

- [1] Souza Filho IR, Ma Y, Kulse M, et al. Sustainable steel through hydrogen plasma reduction of iron ore: process, kinetics, microstructure, chemistry. *Acta Mater.* 2021;213:116971, doi:10.1016/j.actamat.2021.116971.
- [2] European Climate Law (no date). *Climate action*. [cited October 21, 2022]. Available from: https://climate.ec.europa.eu/eu-action/european-green-deal/european-climate-law_en.
- [3] Soni KN, Thakkar JR. Hydrogen Plasma Smelting Reduction: An Option for Steelmaking In The Future. *Int J Res Appl Sci Eng Technol (IJRASET)*. 2017;5(9):839–848. doi:10.22214/ijraset.2017.9124.
- [4] Hasanbeigi A, Arens M, Price L. *Renew Sustain Energ Rev.* 2014;33:645–658. doi:10.1016/j.rser.2014.02.031.
- [5] Junjie Y. Progress and future of breakthrough low-carbon steelmaking technology (ULCOS) of EU. *Int J Mineral Process Extractive Metall.* 2018;3(2):15–22. doi:10.11648/j.ijmpem.20180302.11.
- [6] Bellevrat E, Menanteau P. Introducing carbon constraint in the steel sector: ULCOS scenarios and economic modeling. *Revue de Métallurgie.* 2009;9:318–324. doi:10.1051/metal/2009059.
- [7] Meijer K, Zeilstra C, Teerhuis C, et al. Developments in alternative ironmaking. *Trans Indian Inst Met.* 2013;66:475–481. doi:10.1007/s12666-013-0309-z.
- [8] Van der Stel J, Meijer K, Santos S, et al. (2017). Hisarna, an opportunity for reducing CO₂ emissions from steel industry.
- [9] Pei M, Petajaniemi M, Regnell A, et al. Toward a fossil free future with HYBRIT: development of iron and steelmaking technology in Sweden and Finland. *Metals.* 2020;10(7):972, doi:10.3390/met10070972.
- [10] Tang J, Chu M, Li F, et al. Development and progress on hydrogen metallurgy. *Int J Minerals, Metallurgy Mater.* 2020;27(6):713–723. doi:10.1007/s12613-020-2021-4.
- [11] Kawasaki E, Sanscrainte J, Walsh TJ. Kinetics of reduction of iron oxide with carbon monoxide and hydrogen. *AIChE J.* 1962;8(1):48–52. doi:10.1002/aic.690080114.
- [12] Lin H-Y, Chen Y-W, Li C. The mechanism of reduction of iron oxide by hydrogen. *Thermochim Acta.* 2003;400(1–2):61–67. doi:10.1016/S0040-6031(02)00478-1.
- [13] Qie Y, Lyu Q, Li J, et al. Effect of hydrogen addition on reduction kinetics of iron oxides in Gas-injection BF. *ISIJ Int.* 2017;57(3):404–412. doi:10.2355/isijinternational.ISIJINT-2016-356.
- [14] Ban-ya S, Iguchi Y, Nagasaka T. Rate of reduction of liquid wustite with hydrogen. *Tetsu-to-Hagane.* 1984;70(14):1689–1696. doi:10.2355/tetsutohagane1955.70.14_1689.
- [15] Nagasaka T, Hino M, Ban-Ya S. Interfacial kinetics of hydrogen with liquid slag containing iron oxide. *Metall Mater Trans B.* 2000;31(5):945–955. doi:10.1007/s11663-000-0071-6.
- [16] Naseri Seftejani M, Schenk J, Zarl MA. Reduction of haematite using hydrogen thermal plasma. *Materials.* 2019;12(10):1608, doi:10.3390/ma12101608.
- [17] Kamiya K, Kitahara N, Morinaka I, et al. Reduction of molten iron oxide and FeO bearing slags by H₂-Ar plasma. *Trans Iron Steel Inst Japan.* 1984;24(1):7–16.
- [18] Khasraw D, Yan Z, Hage JLT, et al. Reduction of FeO in molten slag by solid carbonaceous materials for Hisarna alternative ironmaking process. *Metall Mater Trans B.* 2022;53(5):3246–3261. doi:10.1007/s11663-022-02603-5.
- [19] Htet T, Yan Z, Khasraw D, et al. *Metall Mater Trans B.* 2022;54:868–879.
- [20] Fruehan RJ, Martonik LJ. The rate of decarburization of liquid iron by CO₂ and H₂. *Metall Mater Trans B.* 1974;5(5):1027–1032. doi:10.1007/BF02644314.
- [21] Seetharaman S, McLean A, Guthrie R, et al. *Treatise on process metallurgy.* Oxford: Elsevier; 2014, pp.143–177.
- [22] Sasai K, Mizukami Y. Oxidation rate of molten steel by argon Gas blowing in tundish oxidizing atmosphere. *ISIJ Int.* 2011;51(7):1119–1125. doi:10.2355/isijinternational.51.1119.
- [23] Gunji K. Kinetics of decarburization of liquid iron in an oxidizing atmosphere. *Trans Iron Steel Inst Japan.* 1970;10(1):1–12. doi:10.2355/isijinternational1966.10.1.
- [24] Vyazovkin S, Burnham AK, Criado JM, et al. ICTAC kinetics committee recommendations for performing kinetic computations on thermal analysis data. *Thermochim Acta.* 2011;520(1):1–19.
- [25] Bamford CH, Tipper CFH. *Comprehensive chemical kinetics: reactions in the solid state.* 1980;22:41–71.
- [26] Huaiwei Z, Xiaoyan S, Bo Z, et al. Reduction of molten copper slags with mixed CO-CH₄-Ar Gas. *Metall Mater Trans B.* 2013;45(2):582–589. doi:10.1007/s11663-013-9981-y.
- [27] Ouyang K, Dou Z, Zhang T, et al. *J Min Metall Sect B.* 2019;55(2):187–196. doi:10.2298/JMMB190121026Y.
- [28] Li B, Wang X, Wang H, et al. Smelting reduction and kinetics analysis of magnetic iron in copper slag using waste cooking oil. *Sci Rep.* 2017;7(1):2406, doi:10.1038/s41598-017-02696-y.
- [29] Mishra K, Kapoor M. Kinetics of liquid-gas reactions through bubbles. *Hydrometallurgy.* 1978;3(1):75–83. doi:10.1016/0304-386X(78)90008-7.
- [30] Gulliver J. *Introduction to chemical transport in the environment.* Cambridge: Cambridge University Press; 2012, pp.213–215.
- [31] Mills K. *Southern African Pyrometallurgy.* 2011;52:1–56.
- [32] Subramanian R. *Convective Mass Transfer,* 2022. [online] Web2.clarkson.edu. [cited 22 September 2022]. Available from: <<https://web2.clarkson.edu/projects/subramanian/ch330/notes/Convective%20Mass%20Transfer.pdf>>.